Supplementary material for:

Simultaneous thickness and thermal conductivity measurements of thinned silicon from 100 nanometers to 17 microns

Ethan A. Scott,[1,2] Christopher Perez,[1,3] Christopher Saltonstall,[1] David P. Adams,[1] V. Carter Hodges,[1] Mehdi Asheghi,[3] Kenneth E. Goodson,[3] Patrick E. Hopkins,[2,4,5] Darin Leonhardt,[1] and Elbara Ziade[1]

[1)]*Sandia National Laboratories, Albuquerque, NM 87185, USA*

[2)]*Deptartment of Mechanical and Aerospace Engineering, University of Virginia, Charlottesville, VA 22904, USA*

[3)]*Department of Mechanical Engineering, Stanford University, Palo Alto, California 94305*

[4)]*Deptartment of Materials Science and Engineering, University of Virginia, Charlottesville, VA 22904, USA*

[5)]*Department of Physics, University of Virginia, Charlottesville, VA 22904, USA*

CONTENTS

S1. Parameters used in thermal model 3

S2. Sensitivity analysis 5

S3. Thermal Resistance 6

S4. Thin film thermal conductivity models 8

S5. Additional Thermal Conductivity Measurements 10

References 11

S1. PARAMETERS USED IN THERMAL MODEL

The thickness and thermal conductivity of the transducer layer are determined from measurements on a witness sample of SiO_2 included in the same Ti/Au deposition as the thinned silicon. The thermal conductivity and thickness of the thinned silicon layer are treated as fitting parameters within the model, while the volumetric heat capacity is independent of thickness, and is referenced from literature[1–3]. The Ti is considered as part of the interfacial resistance between the transducer and subsequent layer as opposed to an individual layer. Given the thinness of the Ti relative to the Al, the two PVD metal layers are considered as a single continuum in the same manner. For the thermal conductivity of the layer, we assume a value of 100 W m^{-1} K^{-1}, which is typical of evaporatively deposited Al films[2,4]. Furthermore, we apply a literature value of 2.43 MJ m^{-3} K^{-1} for the volumetric heat capacity, often used for Al films[2,5,6]. For the epoxy, a value of 0.3 W m^{-1} K^{-1} is assumed for the thermal conductivity[7], and 2 MJ m^{-3} K^{-1} the volumetric heat capacity, which is typical of fully cured epoxy resins[8,9].

We note that due to the low thermal conductivity and large thickness of the epoxy layer, it can be considered a semi infinite medium, beneath which, there is no sensitivity to the underlying silicon. For example, the thermal penetration depth of a modulated heat source can be approximated, to first order, as:

$$\delta = \sqrt{\kappa/(\pi \rho c_p f)}, \tag{S1}$$

where δ is the 1/e depth of thermal penetration (i.e., the depth at which the induced temperature rise is 1/e that of the surface), ρc_p is the volumetric heat capacity, and f is the modulation frequency of the pump[10]. At the lowest modulation frequency, 1 kHz, and assuming the modulated heat source were at the surface of the epoxy, the upper bound of the thermal penetration depth would be approximately 8.4 μm. This is an overestimation of the actual thermal penetration depth within the material as it does not account for the attenuation of the temperature rise caused by the layers and interfaces atop the epoxy nor spot size[10]. Given that the epoxy is measured to be 98 μm, there are negligible effects from the epoxy/substrate interface and silicon substrate, and therefore consider the epoxy as a semi-infinite substrate in the thermal model.

With the initial FDTR measurements (Fig. 3a of the main manuscript), that data is first fit with d_2, κ_2 and G_1 (the thermal boundary conductance of Au/Ti and silicon interface) as fit parameters. The resultant thermal boundary conductance values of the interface are plotted in Fig S1 for thicknesses spanning approximately 1.5 - 10 μm. There is no observable trend with thickness over the

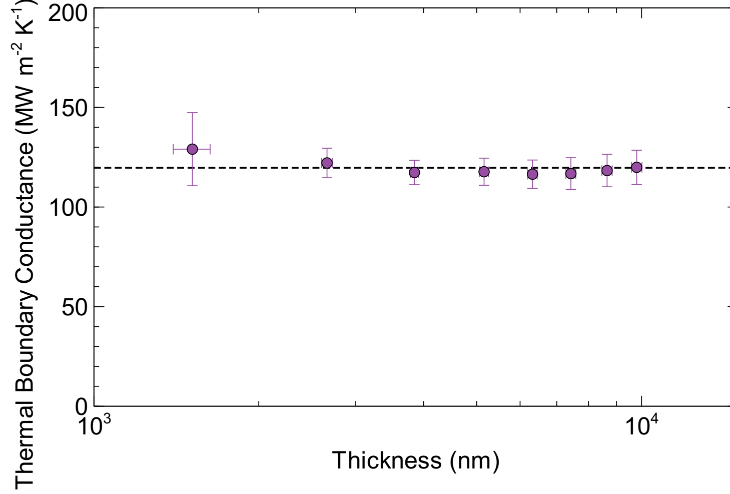

FIG. S1. Measured thermal boundary conductance of the Au/Ti and Si interface (G_1) as a function of Si thickness. The average value over the measured range (120 ± 8.8 MW m^{-2} K^{-1}) is indicated by the black, dashed line.

measured region, and we therefore apply the average value of (120 MW m^{-2} K^{-1}) for subsequent measurements. For the back side interface, we assume a a value 150 MW m^{-2} K^{-1}, which is typical of metal/silicon interfaces[11]. As previously mentioned, we neglect the interface of the Ti/Al layers as metal/metal interfaces have been demonstrated to have significantly lower interfacial resistances as opposed to metal/non-metal interfaces[12,13], and consider the two layers as a single region. Finally, we assume a value of 50 MW m^{-2} K^{-1} for the thermal boundary conductance at the epoxy interfaces, which is an average value within the range of reported silicon/polymer interfaces[14,15].

S2. SENSITIVITY ANALYSIS

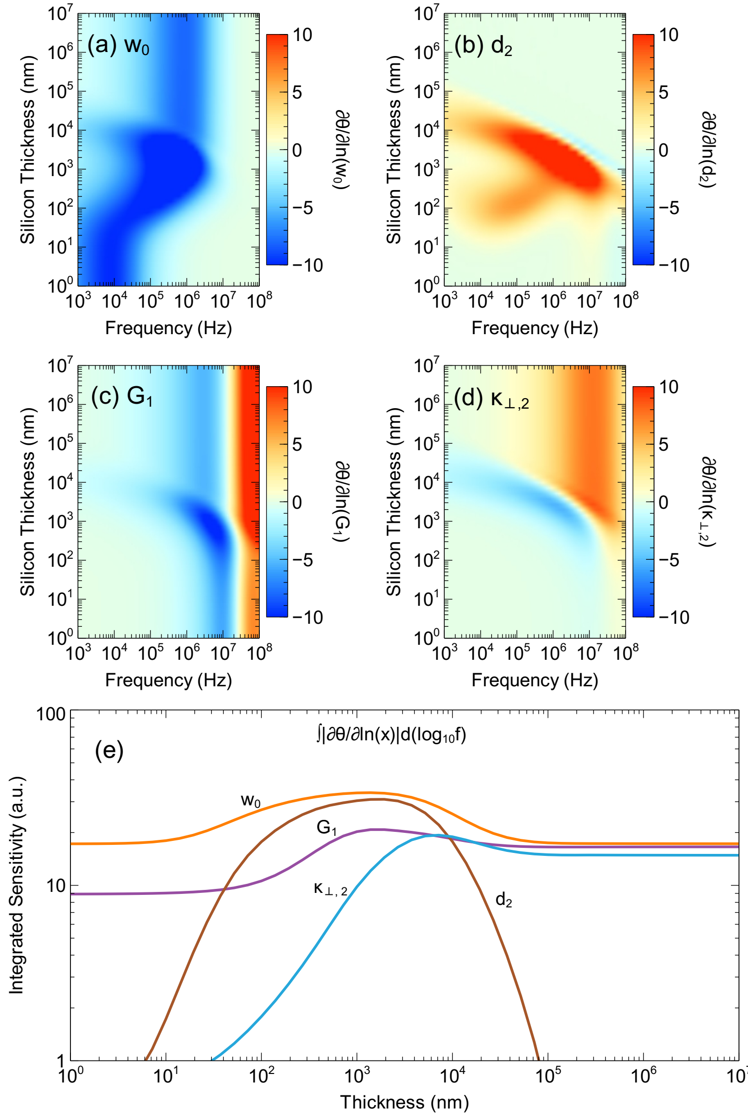

FIG. S2. Contours of the sensitivity for a given parameter, x, as a function of modulation frequency and silicon thickness(a)-(d). In (e) the absolute value of the sensitivity is then integrated as a function of the (log) frequency to provide qualitative insight to the overall sensitivity as a function of thickness. The parameters used here are the same as those tabulated in Table I of the main manuscript; because κ_2 varies with thickness, we assume-thickness-dependent thermal conductivity based upon the model by Callaway[16] in these sensitivity calculations.

S3. THERMAL RESISTANCE

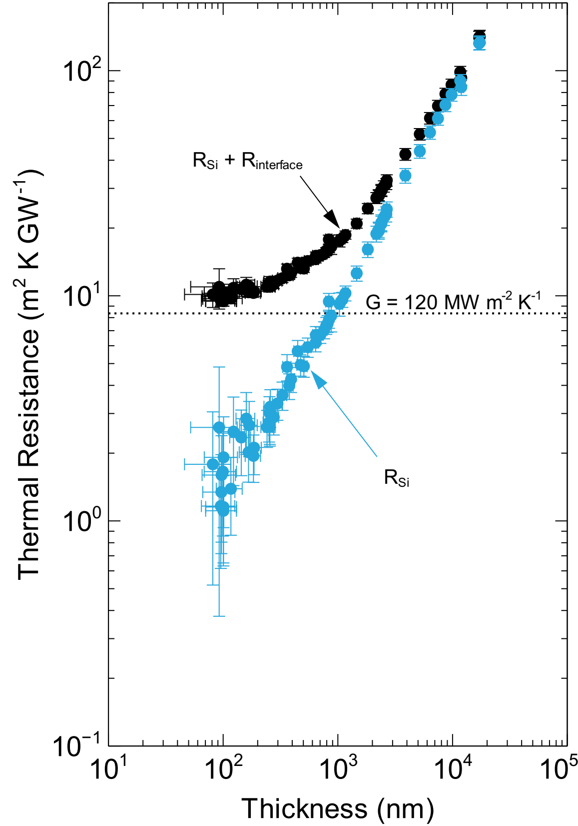

FIG. S3. Intrinsic thermal resistance of the silicon layer, R_{Si}, and combined thermal resistance of the Au/Ti and silicon interface, $R_{Si} + R_{interface}$. The thermal resistance posed by an interface with $G = 120$ MW m^{-2} K^{-1} is displayed by the black, dotted line.

In consideration of measured thermal resistances, we plot the thermal resistance of the silicon wedge as a function of thickness in Fig. S3. The effective resistance of the silicon, R_{Si}, is calculated as $R_{Si} = d_{Si}/\kappa_{Si}$, where d_{Si} and κ_{Si} are the measured thickness and thermal conductivity, respectively. As seen from Fig. S3, there is a near linear relationship between the thermal resistance and thickness. The error bars for the effective thermal resistance are calculated via propagation of uncertainty in both the film thickness and thermal conductivity. In addition to the intrinsic resistance of the silicon layer, we consider the added resistance of the interface between the Ti/Au transducer and the Si. The thermal resistance posed by the interface is calculated as $1/G$, where G is the thermal boundary conductance of the interface. The resistance corresponding to $G = 120$ MW m^{-2} K^{-1} is displayed as the black, dotted line. The intersection of this line

and R_{Si} demonstrates that the interface poses the largest source of thermal resistance for thicknesses less than 1 μm. We additionally plot the cumulative resistance of the film and interface, $R_{Si} + R_{interface}$. The total resistance asymptotes towards the interface resistance in the low thickness extreme, which illustrates high measurement sensitivity to the value of G_1 for very small film thicknesses. In a similar analysis of thin, high-k dielectric films[3], this asymptotic behavior is observed for films approaching 10 nm. In this case, the interface resistance dominates, even at thicknesses up to 1 μm, due to the higher thermal conductivity of the crystalline silicon layer as opposed to an amorphous dielectric film.

S4. THIN FILM THERMAL CONDUCTIVITY MODELS

The measured thermal conductivity of the silicon wedge is compared against several models which consider the reduction in thermal conductivity due to boundary scattering attributed to reduced material dimensions. These analytical models are based upon the approaches of Callaway[16], Holland[17], Born-von Karman-Slack[18,19], and a model considering an experimentally derived phonon dispersion for silicon, determined by Weber[20]. In the case of the thin film models based upon Callaway, thermal conductivity can be expressed as:

$$\kappa = \int_0^{k_B\Theta_D/\hbar} \tau \frac{\hbar^2\omega^2}{k_B^2T^2} \frac{e^{\hbar\omega/k_BT}}{(e^{\hbar\omega/k_BT}-1)^2}\omega^2 d\omega \tag{S2}$$

where k_B is the Boltzmann constant, $\hbar$ is Planck's constant, Θ_D, is the Debye temperature, ω is the phonon frequency, and τ is the relaxation time, which is composed of scattering rates attributed to impurity scattering, Umklapp scattering, and boundary scattering, which are assumed independent, and combined through Matthiessen's rule[16],

$$\tau^{-1} = A\omega^4 + P\omega^2 T e^{-C_U/T} + v/d, \tag{S3}$$

where $A, P,$ and C_U are empirical scattering constants, v is the material's sound speed, and d is the thickness. We note that in this calculation, all scattering terms and parameters are applied from Callaway[16], except we use the correction outlined by Yang and Dames[21] for the Umklapp scattering term to adjust the model for high temperatures.

In the thin film model based upon Holland, which is similar to Callaway, the integral and bounds of integration are separated into different regimes to account for variations in the longitudinal and transverse phonon polarizations as well as $N-$ and $U-$processes[17]. In any case, we utilize the same scattering terms and parameters with the exception of the impurity scattering coefficient, A, which we take as 1.32×10^{-45} s^3 as opposed to the value of 1.32×10^{-44} s^3 reported in the initial work by Holland, which under-predicts the bulk thermal conductivity[17,22,23].

The model based upon the Born-von Karman-Slack formalism is similar to that of Callaway and Holland, however, a sine-type dispersion is assumed rather than Debye or piece-wise linear. In this case, the phonon frequency dispersion can be written as $\omega = \omega_0 \sin(\frac{\pi}{2}\frac{k}{k_0})$, where k is the phonon wave vector, k_0 is the maximum wave vector (1.14×10^{10} m^{-1} (Refs. 21,24)), and ω_0 is defined as $\frac{2}{\pi}v_s k_0$, where v_s is the average sound velocity (6084 m/s). According to Ref. 19, the thickness-dependent thermal conductivity can then be calculated as,

$$\kappa = \frac{\hbar^2}{2\pi^2 k_B T^2} \int_0^{\omega_0} \frac{\omega^2 e^{\frac{\hbar\omega}{k_B T}}}{\left(e^{\frac{\hbar\omega}{k_B T}} - 1\right)^2} \left[\frac{2k_0}{\pi} \sin^{-1}\left(\frac{\omega}{\omega_0}\right)\right]^2 v_g \tau d\omega. \tag{S4}$$

The group velocity is defined as $v_g = d\omega/dk = \frac{\pi}{2k_0}\omega_0 \cos\left(\frac{\pi}{2}\frac{k}{k_0}\right)$. For τ, we utilize the same scattering terms as in Equation S3, using the coefficients provided by Yang and Dames[21].

Furthermore, we consider the thermal conductivity by utilizing the phonon dispersion for silicon reported by Weber[20], which considers the longitudinal and transverse acoustic and optical modes of the first Brillioun zone. We use the same scattering terms defined in Equation S3, and determine the coefficients for A, P and C_U by fitting temperature dependent data (for T $>$ 200 K) from Glassbrenner and Slack[25][21] (and apply a value of 5.7 mm for the thickness), which yields coefficients of 2.74$\times 10^{-45}$ s^3, 1.43$\times 10^{-19}$ s K^{-1}, and 176 K, respectively. The thermal conductivity can be determined by integrating over the phonon wave vector[26]:

$$\kappa = \frac{1}{6\pi^2} \sum_j \int_0^{k_{max}} \frac{\hbar^2 \omega_j^2}{k_B T^2} \frac{e^{\frac{\hbar\omega_j}{k_B T}}}{\left(e^{\frac{\hbar\omega_j}{k_B T}} - 1\right)^2} k^2 v_j^2 \tau_j dk, \tag{S5}$$

where j is an index representing the phonon branch. In this case, each phonon dispersion branch, ω_j, is a function of the wave vector, k, as is the group velocity ($v_j = d\omega_j/dk$). In the calculation of $k_{max} = 2\pi/a$, a is the lattice parameter of silicon (5.43$\times 10^{-10}$ m).

S5. ADDITIONAL THERMAL CONDUCTIVITY MEASUREMENTS

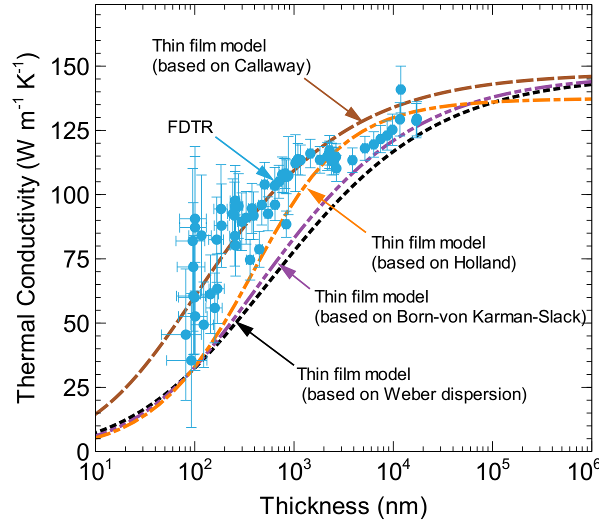

FIG. S4. Thermal conductivity measurements of the wedge as a function of thickness. For comparison, the measurements are plotted with several analytical models for the thickness-dependent thermal conductivity of silicon.

Compared to measured thickness, there is higher uncertainty in the measured thermal conductivity, which is attributed to reduced sensitivity as the film becomes thinner. This gives rise to large uncertainties for films on the order of 100 nm, and for smaller thicknesses, direct measurements can not be made. To improve the precision of the measurement, a swath of measurements were taken and averaged at equal spacings along the gradient. Specifically, we average the thermal conductivity data by grouping measurements into equal, logarithmically spaced bins and take the average value from within each bin, shown in Fig. 3(b) of the main manuscript. The non-averaged results from all measurements are shown in Fig. S4, above.

REFERENCES

[1] J. Yang, E. Ziade, and A. J. Schmidt, "Uncertainty analysis of thermoreflectance measurements," Rev. Sci. Instrum. **87**, 014901 (2016).

[2] E. A. Scott, S. W. Smith, M. D. Henry, C. M. Rost, A. Giri, J. T. Gaskins, S. S. Fields, S. T. Jaszewski, J. F. Ihlefeld, and P. E. Hopkins, "Thermal resistance and heat capacity in hafnium zirconium oxide (Hf1–xZrxO2) dielectrics and ferroelectric thin films," Appl. Phys. Lett. **113**, 192901 (2018).

[3] E. A. Scott, J. T. Gaskins, S. W. King, and P. E. Hopkins, "Thermal conductivity and thermal boundary resistance of atomic layer deposited high-k dielectric aluminum oxide, hafnium oxide, and titanium oxide thin films on silicon," APL Mater. **6**, 058302 (2018).

[4] E. A. Scott, K. Hattar, J. L. Braun, C. M. Rost, J. T. Gaskins, T. Bai, Y. Wang, C. Ganski, M. Goorsky, and P. E. Hopkins, "Orders of magnitude reduction in the thermal conductivity of polycrystalline diamond through carbon, nitrogen, and oxygen ion implantation," Carbon **157**, 97–105 (2020).

[5] E. H. Buyco and F. E. Davis, "Specific heat of aluminum from zero to its melting temperature and beyond. Equation for representation of the specific heat of solids," J. Chem. Eng. Data **15**, 518–523 (1970).

[6] A. Sood, R. Cheaito, T. Bai, H. Kwon, Y. Wang, C. Li, L. Yates, T. Bougher, S. Graham, M. Asheghi, M. Goorsky, and K. E. Goodson, "Direct Visualization of Thermal Conductivity Suppression Due to Enhanced Phonon Scattering Near Individual Grain Boundaries," Nano Lett. **18**, 3466–3472 (2018).

[7] H. Yu, L. Li, T. Kido, G. Xi, G. Xu, and F. Guo, "Thermal and insulating properties of epoxy/aluminum nitride composites used for thermal interface material," J. Appl. Polym. Sci. **124**, 669–677 (2012).

[8] J. McHugh, P. Fideu, A. Herrmann, and W. Stark, "Determination and review of specific heat capacity measurements during isothermal cure of an epoxy using TM-DSC and standard DSC techniques," Polym. Test. **29**, 759–765 (2010).

[9] G. Kalogiannakis, D. Van Hemelrijck, and G. Van Assche, "Measurements of Thermal Properties of Carbon/Epoxy and Glass/Epoxy using Modulated Temperature Differential Scanning Calorimetry," J. Compos. Mater. **38**, 163–175 (2004).

[10] J. L. Braun and P. E. Hopkins, "Upper limit to the thermal penetration depth during modulated

heating of multilayer thin films with pulsed and continuous wave lasers: A numerical study," J. Appl. Phys. **121**, 175107 (2017).

[11]R. Cheaito, J. T. Gaskins, M. E. Caplan, B. F. Donovan, B. M. Foley, A. Giri, J. C. Duda, C. J. Szwejkowski, C. Constantin, H. J. Brown-Shaklee, J. F. Ihlefeld, and P. E. Hopkins, "Thermal boundary conductance accumulation and interfacial phonon transmission: Measurements and theory," Phys. Rev. B **91**, 035432 (2015).

[12]R. Cheaito, K. Hattar, J. T. Gaskins, A. K. Yadav, J. C. Duda, T. E. Beechem, J. F. Ihlefeld, E. S. Piekos, J. K. Baldwin, A. Misra, and P. E. Hopkins, "Thermal flux limited electron Kapitza conductance in copper-niobium multilayers," Appl. Phys. Lett. **106**, 093114 (2015).

[13]B. C. Gundrum, D. G. Cahill, and R. S. Averback, "Thermal conductance of metal-metal interfaces," Phys. Rev. B **72**, 245426 (2005).

[14]J. Liu, S. Ju, Y. Ding, and R. Yang, "Size effect on the thermal conductivity of ultrathin polystyrene films," Appl. Phys. Lett. **104**, 153110 (2014).

[15]E. Ziade, M. Goni, T. Sato, P. Czubarow, and A. J. Schmidt, "Thermal conductance of nanoscale Langmuir-Blodgett films," Appl. Phys. Lett. **107**, 221603 (2015).

[16]J. Callaway, "Model for Lattice Thermal Conductivity at Low Temperatures," Phys. Rev. **113**, 1046–1051 (1959).

[17]M. G. Holland, "Analysis of Lattice Thermal Conductivity," Phys. Rev. **132**, 2461–2471 (1963).

[18]B. Feng, Z. Li, and X. Zhang, "Prediction of size effect on thermal conductivity of nanoscale metallic films," Thin Solid Films **517**, 2803–2807 (2009).

[19]Y. Murakami, H. Goto, Y. Taguchi, and Y. Nagasaka, "Measurement of Out-of-Plane Thermal Conductivity of Epitaxial YBa2Cu3O7-δThin Films in the Temperature Range from 10 K to 300 K by Photothermal Reflectance," Int. J. Thermophys. **38**, 160–22 (2017).

[20]W. Weber, "Adiabatic bond charge model for the phonons in diamond, Si, Ge, and $\alpha - \mathrm{Sn}$," Phys. Rev. B **15**, 4789–4803 (1977).

[21]F. Yang and C. Dames, "Mean free path spectra as a tool to understand thermal conductivity in bulk and nanostructures," Phys. Rev. B **87**, 035437 (2013).

[22]R. Ma, *Examination Of Callaway-Holland-Based ThermalConductivity Calculation For Nano-PhononicCrystals*, Ph.D. thesis, University of Pennsylvania (2018).

[23]R. P. Chhabra, *CRC Handbook of Thermal Engineering* (CRC Press, 2017).

[24]C. Dames and G. Chen, "Theoretical phonon thermal conductivity of Si/Ge superlattice nanowires," J. Appl. Phys. **95**, 682–693 (2004).

[25]C. J. Glassbrenner and G. A. Slack, "Thermal Conductivity of Silicon and Germanium from 3 K to the Melting Point," Phys. Rev. **134**, A1058–A1069 (1964).

[26]E. Ziade, J. Yang, G. Brummer, D. Nothern, T. Moustakas, and A. J. Schmidt, "Thickness dependent thermal conductivity of gallium nitride," Appl. Phys. Lett. **110**, 031903 (2017).